

Peng Li · Feng Jin

# Excitation and propagation of shear horizontal waves in a piezoelectric layer imperfectly bonded to a metal or elastic substrate

Received: 4 December 2013 / Revised: 14 May 2014 / Published online: 15 June 2014  
© Springer-Verlag Wien 2014

**Abstract** The performance of shear horizontal waves excited by an external voltage imposed on the surface of a transversely isotropic piezoelectric sensitive layer imperfectly bonded to a metal or elastic substrate is investigated. The phase velocity, electromechanical coupling factor, temperature coefficient of delay, mass loading sensitivity, and displacement distribution along the thickness direction for the propagation of free waves, resonance frequency, and displacement signal and input admittance for the forced vibration are considered. Numerically, the SH wave speed smaller than Bleustein–Gulyaev wave velocity of a piezoelectric layer can be achieved for electrically open and shorted conditions when the interface is imperfect, which is totally different from the case of perfect interface. The imperfect interface evidently improves the energy transformation ratio, temperature stability, and mass sensitivity of the composite structure. The viscoelastic damping parameter has no relationship with resonance frequencies, and it only decreases the amplitudes of displacement signal and input admittance. The outcome is widely applicable and can be used to design high-performance surface acoustic wave devices.

## 1 Introduction

Love waves [1] and Bleustein–Gulyaev (B–G) waves [2,3], which are collectively known as shear horizontal (SH) waves, have been applied widely in sensing and micro-acoustic devices because of the concentration of acoustic energy within a few wavelengths near the surface. Only one relatively simple displacement component exists, thus making wave excitation convenient [4]. In general, a typical layer/substrate configuration form is adopted to achieve high performance. The basic configuration that supports propagation of SH waves consists of a layer deposited on a substrate [5]. In the simplest case, the layer and the substrate are both isotropic media. A piezoelectric material is chosen as the upper sensitive layer to enable electric excitation of SH waves [6,7].

The propagation of SH waves in a piezoelectric layer embedded in a half-space has been investigated extensively, including the influence of boundary conditions [8], electromagnetic coupling characteristics [9], initial stress [10], graded functional material [11,12], dissipation [13], viscous liquid effect [14], and porous material [15].

The aforementioned studies are based on the assumption that the layer is perfectly bonded to the substrate. However, imperfect bonding often occurs in surface acoustic wave (SAW) devices because of the aging of glue applied to two conjunct solids, microdefects, diffusion impurities, and other forms of damages. Hence, two dissimilar materials cannot be perfectly bonded, and an interphase or transition with a thickness typically within the range of 30–240 nm exists across the interface [16]. In the design and application of piezoelectric sensors,

---

P. Li · F. Jin (✉)  
State Key Laboratory for Strength and Vibration of Mechanical Structures, School of Aerospace, Xi'an Jiaotong University,  
Xi'an 710049, People's Republic of China  
E-mail: jinfengzhao@263.net  
Tel.: +86-29-82667091

considering a possible imperfect interface is necessary. The interphase or transition layer is generally very thin, such that it is considered as a middle layer with zero thickness; however, this layer still possesses elasticity and interface elastic strain energy (i.e., the shear-lag model) [17]. The tangential displacement components on both sides of the interface are allowed to be different to account for the deformation of the interface layer. The spring-type relation [18, 19] is also sometimes used to characterize the imperfect interface, in which the effects of such interface on mechanical energy and electric fields are considered. Aside from using the preceding models to investigate theoretically the effect of imperfect interfaces on the propagation of SH waves, Jin et al. [20] and Lavrentyev et al. [21] also performed experimental measurements. More methods that deal with imperfect interfaces can be found in the review article [22].

In the present study, the classical shear-lag model is used to simulate the effect of an imperfect interface on SH wave propagation excited by an external voltage imposed on a piezoelectric sensitive layer. Based on the governing equations, boundary, and continuity conditions, exact solutions that can be reduced to the previous results for several special cases are presented within the context of linear theory of piezoelectricity. The effects of an imperfect interface on the performance of SH waves are investigated, including those on phase velocity, electromechanical coupling factor, temperature coefficient of delay (TCD), mass loading sensitivity, and displacement distribution for the propagation of free waves, resonance frequency, displacement signal, and input admittance for the excited forced vibration. Finally, several conclusions are drawn.

## 2 Statement of the problem and the solutions

Consider the structure of a piezoelectric layer imperfectly bonded to an elastic or metal substrate shown in Fig. 1. In general, the thickness of the substrate is significantly larger than those of the layer and the wavelength for SAW devices, such that it can be treated as a half-space. The upper sensitive layer consists of transversely isotropic piezoelectric materials poled along the  $x_3$  direction and determined from  $x_1$  and  $x_2$  by the right-hand rule. Two electrodes are found on the two surfaces of this layer:  $x_2 = -h$  and 0. The piezoelectric layer is driven by an alternating voltage across the electrodes. Given the specific orientations of the poling direction and the applied electric field, shear horizontal or anti-plane waves that propagate in the positive  $x_1$  direction and penetrate the  $x_2$  direction are generated in this structure [10–15]. Hence,

$$u_1 = u_2 = 0, \quad u_3 = u(x_1, x_2, t), \quad \varphi = \varphi(x_1, x_2, t). \quad (1)$$

The linear piezoelectric constitutive equations can be expressed as [23]

$$\begin{aligned} \sigma_{ij} &= c_{ijkl}u_{k,l} + e_{lij}\varphi_{,l}, \\ D_i &= e_{ikl}u_{k,l} - \varepsilon_{il}\varphi_{,l} \end{aligned} \quad (2)$$

where  $\sigma_{ij}$  and  $D_i$  are the stress tensors and the electrical displacement vector, respectively; and  $c_{ijkl}$ ,  $e_{lij}$ , and  $\varepsilon_{il}$  are the elastic coefficient, the piezoelectric coefficient, and the dielectric permittivity, respectively. An index after a comma denotes partial differentiation with respect to the coordinate.

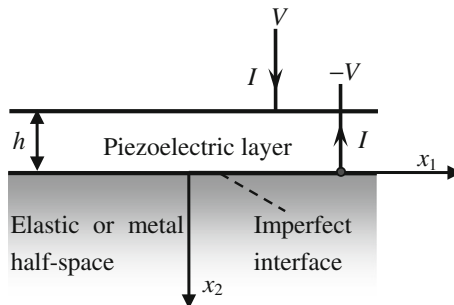


**Fig. 1** Schematic of the composite structure and the Cartesian coordinate system

## 2.1 Solutions for the substrate $x_2 > 0$

The governing equation for shear horizontal or anti-plane vibration in the substrate  $x_2 > 0$  is [14, 15]:

$$\mu \nabla^2 u = \rho \ddot{u}, \quad (3)$$

where  $\mu$  and  $\rho$  are the shear modulus and the mass density of the substrate, respectively;  $\nabla^2 = \partial^2/\partial x_1^2 + \partial^2/\partial x_2^2$  is the 2D Laplacian; and the dot means the time derivative. Given that displacement and stress are finite when  $x_2$  approaches infinity, then the solution for the SH wave propagating in the positive  $x_1$  direction can be expressed as

$$u = C_1 \exp(-kb'x_2) \exp[ik(x_1 - ct)] \quad (4)$$

where  $C_1$  is an undetermined constant,  $t$  is the time,  $b' = \sqrt{1 - (c/c_{\text{sub}})^2}$  is a non-dimensional number, and  $k$  is the wave number in the  $x_1$  direction.  $c_{\text{sub}} = \sqrt{\mu/\rho}$  is the bulk shear velocity in the substrate. Using Eq. (2), the stress component  $\sigma_{32}$  can be obtained as follows:

$$\sigma_{32} = -kb' \mu C_1 \exp(-kb'x_2) \exp[ik(x_1 - ct)]. \quad (5)$$

## 2.2 Solutions for the piezoelectric layer $-h < x_2 < 0$

With the displacement and potential function expressed in Eq. (1), the governing equations for the transversely isotropic piezoelectric sensitive layer are given by [19, 23]:

$$\begin{cases} c_{44} \nabla^2 u + e_{15} \nabla^2 \varphi = \rho_0 \ddot{u} \\ e_{15} \nabla^2 u - \varepsilon_{11} \nabla^2 \varphi = 0 \end{cases} \quad (6)$$

The SH wave solution in the sensitive layer can also be expressed as

$$\begin{aligned} u &= [A_1 \cosh(kbx_2) + A_2 \sinh(kbx_2)] \exp[ik(x_1 - ct)], \\ \varphi &= \left\{ \frac{e_{15}}{\varepsilon_{11}} [A_1 \cosh(kbx_2) + A_2 \sinh(kbx_2)] + [B_1 \cosh(kx_2) + B_2 \sinh(kx_2)] \right\} \exp[ik(x_1 - ct)] \end{aligned} \quad (7)$$

where  $A_1$ ,  $A_2$ ,  $B_1$ , and  $B_2$  are undetermined constants; and  $b = \sqrt{1 - (c/c_{\text{layer}})^2}$  is another non-dimensional number.  $c_{\text{layer}} = \sqrt{\bar{c}_{44}/\rho_0}$  is the bulk shear velocity in the layer with the relative piezoelectric stiffness of  $\bar{c}_{44} = c_{44} + \frac{e_{15}^2}{\varepsilon_{11}}$ . At this point, we assume that the excited SH wave velocity is smaller than the bulk shear velocities of the layer and the substrate (i.e.,  $c < c_{\text{layer}} < c_{\text{sub}}$ ). This wave can sometimes be considered as a B-G wave [4]. If the excited SH wave is a Love wave, i.e.,  $c_{\text{layer}} < c < c_{\text{sub}}$ , then the displacement and potential function can be expressed as

$$\begin{aligned} u &= [A_1 \cos(kbx_2) + A_2 \sin(kbx_2)] \exp[ik(x_1 - ct)] \\ \varphi &= \left\{ \frac{e_{15}}{\varepsilon_{11}} [A_1 \cos(kbx_2) + A_2 \sin(kbx_2)] + [B_1 \cosh(kx_2) + B_2 \sinh(kx_2)] \right\} \exp[ik(x_1 - ct)] \end{aligned} \quad (8)$$

with the non-dimensional number  $b = \sqrt{(c/c_{\text{layer}})^2 - 1}$ . In the following sections, only Eq. (7), i.e.,  $c < c_{\text{layer}} < c_{\text{sub}}$ , is used to complete the following theoretical analysis for simplification. Hence, the corresponding stress and electric displacement components are as follows:

$$\begin{aligned} \sigma_{32} &= \{\bar{c}_{44} kb [A_1 \sinh(kbx_2) + A_2 \cosh(kbx_2)] + e_{15} k [B_1 \sinh(kx_2) + B_2 \cosh(kx_2)]\} \exp[ik(x_1 - ct)], \\ D_2 &= -\varepsilon_{11} k [B_1 \sinh(kx_2) + B_2 \cosh(kx_2)] \exp[ik(x_1 - ct)]. \end{aligned} \quad (9)$$

### 2.3 Vibration solutions

The traction-free surface at  $x_2 = -h$  requires the following:

$$\sigma_{32}(-h) = 0, \quad (10)$$

and the electric potential on this surface satisfies the following:

$$\varphi(-h) = V. \quad (11)$$

At the interface  $x_2 = 0$ , another electrode that can avoid the electric field in the half-space affected by the piezoelectric layer is present. Hence,

$$\varphi(0) = -V. \quad (12)$$

For a perfect bonding case at the joint  $x_2 = 0$  between the layer and the substrate, the continuity of mechanical components  $u$  and  $\sigma_{32}$  must be imposed [8–15]. In this research, however, the joint is regarded as an imperfect bonding in which we use the following shear-lag model:

$$\sigma_{32}(0^+) = \sigma_{32}(0^-) = R [u(0^+) - u(0^-)], \quad (13)$$

in which the tangential displacement at the interface is allowed to be different from both of its sides to account for its deformation. When  $R = 0$ , the two parts lose their mechanical interaction, and the case of  $R = \infty$  is for the perfect interface with a continuous displacement across the joint [16–21]. By substituting displacement, stress, and potential expressions, i.e., Eqs. (4), (5), (7) and (9) into the continuity and boundary conditions, Eqs. (10)–(13) yield five linear homogeneous algebraic equations for coefficients  $A_1$ ,  $A_2$ ,  $B_1$ ,  $B_2$ , and  $C_1$ , as follows:

$$\begin{cases} \frac{e_{15}}{\varepsilon_{11}} [A_1 \cosh(kbh) - A_2 \sinh(kbh)] + [B_1 \cosh(kh) - B_2 \sinh(kh)] = V \\ \bar{c}_{44} b [-A_1 \sinh(kbh) + A_2 \cosh(kbh)] + e_{15} [-B_1 \sinh(kh) + B_2 \cosh(kh)] = 0 \\ \frac{e_{15}}{\varepsilon_{11}} A_1 + B_1 = -V \\ bA_2 + \frac{e_{15}}{\bar{c}_{44}} B_2 + \frac{\mu}{\bar{c}_{44}} b' C_1 = 0 \\ -A_1 + (1 + b' \Gamma) C_1 = 0. \end{cases} \quad (14)$$

We can obtain the solutions as

$$\begin{aligned} A_1 &= \frac{\Delta_1}{\Delta} \cdot \frac{e_{15}}{\bar{c}_{44}} V, \quad A_2 = \frac{\Delta_2}{\Delta} \cdot \frac{e_{15}}{\bar{c}_{44}} V, \quad B_1 = - \left( 1 + k_e^2 \frac{\Delta_1}{\Delta} \right) V, \\ B_2 &= - \left( \frac{\mu b'}{\bar{c}_{44} (1 + b' \Gamma)} \cdot \frac{\Delta_1}{\Delta} + b \frac{\Delta_2}{\Delta} \right) V, \quad C_1 = \frac{\Delta_1}{\Delta (1 + b' \Gamma)} \cdot \frac{e_{15}}{\bar{c}_{44}} V \end{aligned} \quad (15)$$

where

$$\begin{aligned} \Delta &= 2k_e^2 b \left[ \frac{1}{\cosh(kbh) \cosh(kh)} - 1 \right] + (k_e^4 + b^2) \tanh(kbh) \tanh(kh) \\ &\quad + \frac{\mu b'}{\bar{c}_{44} (1 + b' \Gamma)} [b \tanh(kh) - k_e^2 \tanh(kbh)], \end{aligned} \quad (16.1)$$

$$\Delta_1 = b \left[ 1 + \frac{1}{\cosh(kh)} \right] \left[ 1 - \frac{\cosh(kh)}{\cosh(kbh)} \right] + \tanh(kh) \left[ -k_e^2 \tanh(kbh) + b \frac{\sinh(kh)}{\cosh(kbh)} \right], \quad (16.2)$$

$$\begin{aligned} \Delta_2 &= \left[ 1 + \frac{1}{\cosh(kh)} \right] \left[ b \tanh(kbh) - k_e^2 \frac{\sinh(kh)}{\cosh(kbh)} + \frac{\mu b'}{\bar{c}_{44} (1 + b' \Gamma)} \frac{\cosh(kh)}{\cosh(kbh)} \right] \\ &\quad - \tanh(kh) \left\{ k_e^2 \left[ 1 - \frac{\cosh(kh)}{\cosh(kbh)} \right] + \frac{\mu b'}{\bar{c}_{44} (1 + b' \Gamma)} \frac{\sinh(kh)}{\cosh(kbh)} \right\} \end{aligned} \quad (16.3)$$

where  $k_e^2 = e_{15}^2 / (\varepsilon_{11} \bar{c}_{44})$  is the piezoelectric coupling coefficient of the piezoelectric material,  $\Gamma = \frac{k\mu}{R}$  is a non-dimensional number that describes how effectively the sensitive layer and the substrate are bonded, and

$\Gamma = 0$  is for the perfect interface. If the SH wave is a Love wave (i.e.,  $c_{\text{layer}} < c < c_{\text{sub}}$ ), then Eq. (16) can be changed into the following:

$$\Delta = 2k_e^2 b \left[ \frac{1}{\cos(kbh) \cosh(kh)} - 1 \right] + (k_e^4 - b^2) \tan(kbh) \tanh(kh) + \frac{\mu b'}{\bar{c}_{44} (1 + b' \Gamma)} [b \tanh(kh) - k_e^2 \tan(kbh)], \quad (17.1)$$

$$\Delta_1 = b \left[ 1 + \frac{1}{\cosh(kh)} \right] \left[ 1 - \frac{\cosh(kh)}{\cos(kbh)} \right] + \tanh(kh) \left[ -k_e^2 \tan(kbh) + b \frac{\sinh(kh)}{\cos(kbh)} \right], \quad (17.2)$$

$$\Delta_2 = \left[ 1 + \frac{1}{\cosh(kh)} \right] \left[ -b \tan(kbh) - k_e^2 \frac{\sinh(kh)}{\cos(kbh)} + \frac{\mu b'}{\bar{c}_{44} (1 + b' \Gamma)} \frac{\cosh(kh)}{\cos(kbh)} \right] - \tanh(kh) \left\{ k_e^2 \left[ 1 - \frac{\cosh(kh)}{\cos(kbh)} \right] + \frac{\mu b'}{\bar{c}_{44} (1 + b' \Gamma)} \frac{\sinh(kh)}{\cos(kbh)} \right\}. \quad (17.3)$$

### 3 Propagating SH waves

$\Delta = 0$  yields the phase velocity equation of SH wave propagation in the composite structure used in this study when the upper surface is electrically shorted (i.e., without the initial voltage  $V = 0$ ), which is related to the free vibration of such composites,

$$2k_e^2 b \left[ \frac{1}{\cosh(kbh) \cosh(kh)} - 1 \right] + (k_e^4 + b^2) \tanh(kbh) \tanh(kh) + \frac{\mu b'}{\bar{c}_{44} (1 + b' \Gamma)} [b \tanh(kh) - k_e^2 \tanh(kbh)] = 0, \quad (c < c_{\text{layer}} < c_{\text{sub}}), \quad (18.1)$$

$$2k_e^2 b \left[ \frac{1}{\cos(kbh) \cosh(kh)} - 1 \right] + (k_e^4 - b^2) \tan(kbh) \tanh(kh) + \frac{\mu b'}{\bar{c}_{44} (1 + b' \Gamma)} [b \tanh(kh) - k_e^2 \tan(kbh)] = 0, \quad (c_{\text{layer}} < c < c_{\text{sub}}). \quad (18.2)$$

Equation (18) has the same expressions as those in the work of Liu et al. [24]. For the electrically open case, the upper surface of the layer is in the air, and there is no electrode on the upper surface  $x_2 = -h$ ; the electric boundary condition satisfies [25, 26] the following equation:

$$D_2(-h) = 0. \quad (19)$$

Using this equation, we can obtain the following phase velocity of SH wave propagation along the positive direction of the  $x_1$  axis when the upper surface is electrically open:

$$k_e^2 \tanh(kh) - \frac{\mu b'}{\bar{c}_{44} (1 + b' \Gamma)} - b \tanh(kbh) = 0, \quad (c < c_{\text{layer}} < c_{\text{sub}}), \quad (20.1)$$

$$k_e^2 \tanh(kh) - \frac{\mu b'}{\bar{c}_{44} (1 + b' \Gamma)} + b \tan(kbh) = 0, \quad (c_{\text{layer}} < c < c_{\text{sub}}). \quad (20.2)$$

When  $\Gamma = 0$ , i.e., the two materials are perfectly bonded, Eqs. (18) and (20) can reduce the works of Curtis and Redwood [27] and Qian et al. [25], which validate the accuracy of our theoretical derivation to a certain extent.

If piezoelectricity is ignored, that is,  $k_e^2 = 0$ , then Eqs. (18.2) and (20.2) can also be reduced into the same form, as follows:

$$b \tan(kbh) - \frac{\mu b'}{\bar{c}_{44}} = 0, \quad (c_{\text{layer}} < c < c_{\text{sub}}), \quad (21)$$

which is the classical phase velocity of Love waves [1, 28].

### 3.1 Phase velocity

To date, analytical solutions for the phase velocity of SH waves propagating along the positive direction of the  $x_1$  axis in the composite structure have been obtained. However, the fact that Eqs. (18) and (20) are transcendental equations results in the complexity of the aforementioned problem. Thus, we adopt an iterative procedure for the numerical computations [29]. For an initial value of  $c$ , we evaluate the determinant (presented on the left side of phase velocity) for various values of the unknown quantity. A fixed but small increment is added to this unknown quantity each time until the value of the determinant changes its sign. The ‘‘bisection method’’ is then applied to locate the root correctly [29].

A material system of semi-infinite  $\text{SiO}_2$  substrate with a ZnO layer is considered to study the propagation behavior of shear horizontal waves in the composite structure and to show graphically the effect of an imperfect interface on wave properties. The elastic and piezoelectric constants, the mass density, and the dielectric constants are summarized in Table 1 [30,31].

Figure 2 plots the predicted phase velocities of SH waves as functions of the non-dimensional layer thickness  $kh$  when the upper surface is electrically shorted. The figure shows that the phase velocity of the first mode is initiated at the bulk shear wave velocity of the half-space medium. The phase velocity also approaches the B–G wave velocity of the piezoelectric layer as  $kh$  is increased, regardless of the interface state. This result validates the correctness of the present solutions to a certain extent [24,25,32]. Totally speaking, the interface characteristics do not change the number of wave modes. For example, the fourth mode can be excited in this composite structure when the non-dimensional number  $kh = 10.65$ . This value has no relationship with the non-dimensional interfacial parameter  $\Gamma$ . However, the imperfect interface lowers the total stiffness of the structure used in this study, and thus, it reduces the propagating speed of SH waves. The B–G wave speed at an electrically shorted ZnO half-space is  $c_{\text{B-G}} = c_{\text{layer}}\sqrt{1 - k_e^4} = 2,833.4 \text{ m s}^{-1}$  [2]. With the increase of interfacial parameter  $\Gamma$ , for instance,  $\Gamma$  is larger than 20, the minimum value of phase velocity of the first mode can achieve a value which is smaller than the B–G wave velocity in the piezoelectric layer. This is totally different from the case of perfect interface. The phase velocity in an electrically open case is the same as in Fig. 2, which is not depicted for simplicity.

**Table 1** Material parameters

Material constant	Basic properties		Temperature coefficient $a_1$ ( $10^{-4} \text{ }^\circ\text{C}^{-1}$ )	
	$\text{SiO}_2$	ZnO	$\text{SiO}_2$	ZnO
$c_{44}$ (GPa)	31.2	42.3	1.51	0.21
$e_{15}$ (C/m <sup>2</sup> )		−0.48		
$\varepsilon_{11}$ ( $10^{-11}$ F/m)		0.67		
$\rho$ (kg/m <sup>3</sup> )	2,200	5,665	−0.0165	−0.101

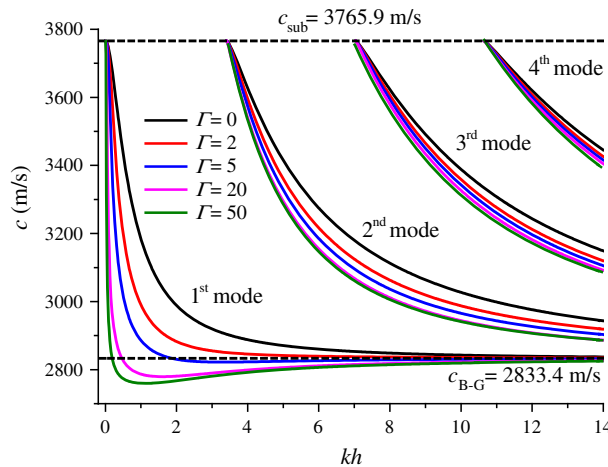


**Fig. 2** The phase velocities of SH waves as functions of the non-dimensional layer thickness  $kh$  when the upper surface is electrically shorted

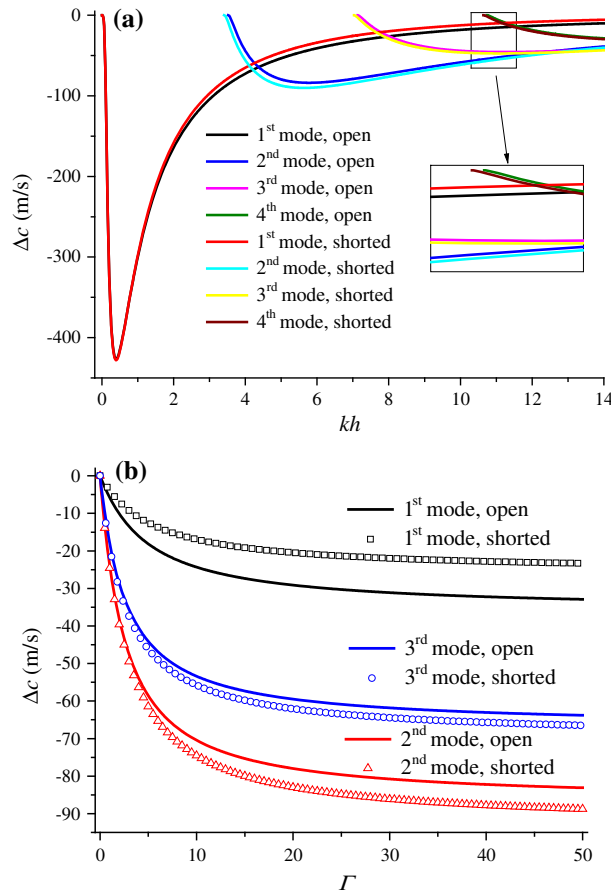


**Fig. 3** The phase velocity change  $\Delta c$  under different conditions: **a** with the non-dimensional layer thickness  $kh$  ( $\Gamma = 5$ ) and **b** with the non-dimensional interface parameter  $\Gamma$  ( $kh = 10$ )

Assuming the phase velocity change  $\Delta c = c - c_0$ , where  $c_0$  stands for the velocity when the interface is perfect, Fig. 3a, b respectively depicts the phase velocity change  $\Delta c$  with  $kh$  and  $\Gamma$  for electrically open and shorted cases. The phase velocity change exhibits the same variation pattern under different electrical conditions. Moreover,  $\Delta c$  is negative because the imperfect interface lowers the stiffness of the substrate-layer structure. The absolute value of velocity shift for the fundamental mode initially increases with increasing dimensional wave number, reaches a maximum, and then decreases and approaches zero at a large  $kh$ . When the interface becomes increasingly weak (i.e.,  $R$  decreases or  $\Gamma$  increases), the phase velocities of all modes initially decrease and then approach a finite value, as shown in Fig. 3b. By considering the limit case of  $R = 0$  or  $\Gamma = \infty$ , then the piezoelectric sensitive layer and the substrate are no longer connected. In this situation, the wave only propagates in the layer and is not affected by the substrate. The speed  $c$  is a finite value that is only related to the non-dimensional number  $kh$  and has no relationship with the interface parameter  $R$  or  $\Gamma$ . This speed can explain why  $\Delta c$  approaches a finite value with increasing  $\Gamma$ .

### 3.2 Electromechanical coupling factor

A high electromechanical coupling factor and a low penetration depth of waves in SAW devices are expected in engineering applications. The electromechanical coupling factor  $K^2$  is defined as [5,25,33]

$$K^2 = \frac{2(c_{\text{open}} - c_{\text{shorted}})}{c_{\text{open}}}, \quad (22)$$

where  $c_{\text{open}}$  and  $c_{\text{shorted}}$  are the phase velocities for the electrically open and electrically shorted cases, respectively. This factor is an important material parameter for designing sensors and is directly related to the

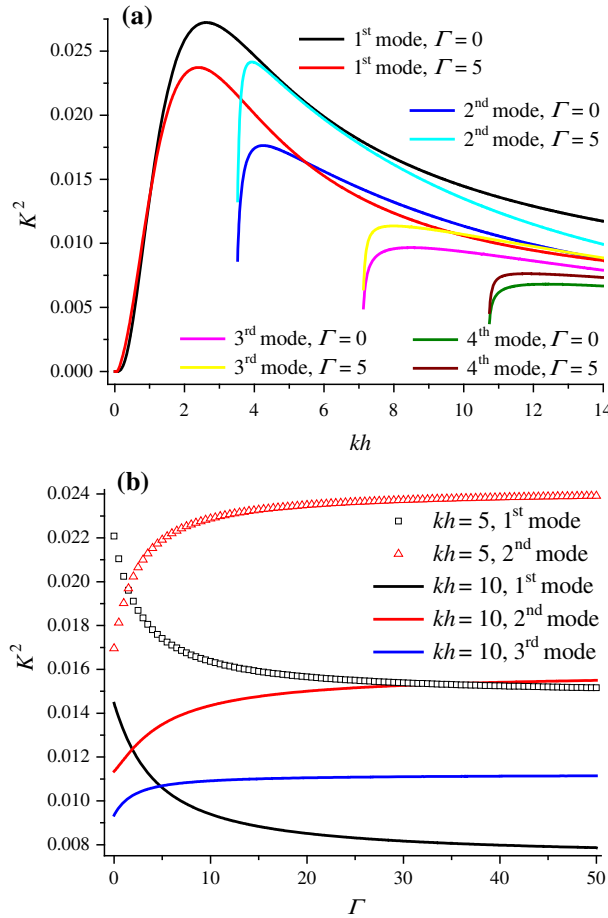


**Fig. 4** The electromechanical coupling factor  $K^2$  under different modes: **a** with the non-dimensional layer thickness  $kh$  ( $\Gamma = 0, 5$ ) and **b** with the non-dimensional interface parameter  $\Gamma$  ( $kh = 10$ )

efficiency of a transducer in converting electrical energy into mechanical energy, and vice versa [33,34]. Emphasizing that the electromechanical coupling factor  $K^2$  is different from the piezoelectric coupling factor  $k_e^2$  mentioned earlier is important. First,  $K^2$  is suitable for any type of wave, including Rayleigh waves, Lamb waves, B–G waves, and Love waves. However,  $k_e^2$  is related to SH waves in a transversely isotropic piezoelectric medium. For other categories of piezoelectric media, the piezoelectric coupling factor has an expression different from that of  $k_e^2$ . Second,  $k_e^2$  can also be used to solve static coupling equations between the mechanical displacement and the electric field. By contrast,  $K^2$  only emerges in dynamic problems. More information on the two parameters is found in Reference [35].

Figure 4a, b shows the electromechanical coupling factor  $K^2$  of SH waves with the non-dimensional layer thickness  $kh$  and the interface parameter  $\Gamma$ , respectively. The imperfect interface strongly influences the electromechanical coupling factor. The energy efficiency of the first mode is reduced during the interference of the imperfect interface. However, this value improves for higher modes with increasing interface parameter  $\Gamma$ . The maximum value of  $K^2$  for a particular mode of SH waves in the ZnO–SiO<sub>2</sub> structure is obtained by choosing  $kh$  and  $\Gamma$  properly. This finding is beneficial to the practical design of SAW devices because the energy conversion efficiency is significantly increased during the propagation of SH waves by choosing the depth of the layer appropriately according to the characteristics of the interface.

### 3.3 The TCD

The effect of temperature on SAW propagation characteristics is typically characterized in terms of the TCD given by [36,37]:

$$\alpha_T = \frac{1}{\tau} \frac{d\tau}{dT} = \frac{1}{L} \frac{dL}{dT} - \frac{1}{c} \frac{dc}{dT}, \quad (23)$$

where  $\tau = L/c$  is the time delay between the input and output interdigital transducers separated by a distance  $L$ ,  $c$  is the SAW phase velocity, and  $T$  is the substrate temperature. The coefficient  $\alpha_T$  expressed in units of  $\text{ppm } ^\circ\text{C}^{-1}$  is independent of transducer separation.  $\alpha_T$  should be as small as possible to fabricate devices with good temperature stability. The first term in Eq. (23) provides the change in TCD caused by thermal expansion or contraction of the substrate material along the SH propagation direction. In case of a layered structure, the difference in the thermal expansion coefficient of various layers and the substrate can lead to thermal strain. For the numerical simulation, the thermal strain for the material combinations considered in the present study is found to be extremely small [37]. Hence, we fix it at zero for convenience [36,37]. The second term relates to the velocity shift caused by changes in temperature and is known as the temperature coefficient of SAW velocity. For the theoretical calculations, TCD is given by [36–38]:

$$\alpha_T = -\frac{c_{35} - c_{15}}{20c_{25}}, \quad (24)$$

where  $c_{15}$ ,  $c_{25}$ , and  $c_{35}$  are the SAW velocities at 15, 25, and 35  $^\circ\text{C}$ , respectively. These values can be calculated by using the material constants (i.e., density, elastic, piezoelectric, and dielectric constants) at a given temperature. The temperature dependence of the material constants is approximated by a second-order function and is expressed as follows [36–39]:

$$X = X_0 [1 + a_1 (T - T_0) + a_2 (T - T_0)^2], \quad (25)$$

where  $X$  is the material constant at each temperature,  $X_0$  is the material constant at room temperature,  $T$  is the temperature,  $T_0$  is the room temperature (25  $^\circ\text{C}$  in this study), and  $a_1$  and  $a_2$  are the first- and second-order temperature coefficients of the material constants, respectively. Given that the second-order temperature coefficient of the material constants ( $a_2$ ) for the materials used in the present layered configurations are hardly achieved, we restrict our analysis to using only first-order temperature coefficients ( $a_1$ ). The temperature coefficients used in the calculations are summarized in Table 1 [36–39].

Figures 5 and 6 show the variation of the TCD with normalized thickness for the ZnO film  $kh$  and the interface parameter  $\Gamma$  for specific cases, respectively. Higher modes have better temperature stability compared with the fundamental mode. However, a zero TCD cannot be achieved in the ZnO/SiO<sub>2</sub> layered structure even if the interface is perfect. This condition occurs because the first-order temperature coefficients ( $a_1$ ) of ZnO and SiO<sub>2</sub> materials have a synchronized effect on SH wave velocity, as shown in Table 1. Relative stiffness is increased by an increment in temperature, and the opposite effect occurs when temperature decreases. Hence, a zero TCD cannot be achieved in this structure. However, an imperfect interface lowers the absolute value of  $\alpha_T$  for all modes of SH waves. This scenario implies that the temperature stability of the composite structure has been improved evidently by the presence of an imperfect interface. Meanwhile, high-frequency short waves have a relatively small absolute TCD value (i.e., good temperature stability) when the interface is weakly bonded, as shown in Figs. 5 and 6.

### 3.4 Mass loading sensitivity

The mass loading sensitivity of an acoustic sensor can be defined as a relative change in phase velocity resulting from mass loading on the surface [37]. Hence,

$$S_c = \frac{1}{c_0} \lim_{\Delta m \rightarrow 0} \frac{c - c_0}{\Delta m}, \quad (26)$$

where  $c_0$  is the phase velocity corresponding to the operation frequency without perturbation,  $c - c_0$  is the change in phase velocity resulting from the mass per unit area  $\Delta m$  deposited on the surface, and  $c$  is the phase velocity after perturbation. A thin silicon layer with thickness  $H$  and  $\rho' = 2,328 \text{ kg m}^{-3}$  is also deposited on top of the structure. In this study, we use this piezoelectric composite structure shown in Fig. 1 to detect the change in thickness of the additional thin silicon layer. Thus [40],

$$S_c \approx \frac{c - c_0}{c_0 H \rho'}. \quad (27)$$

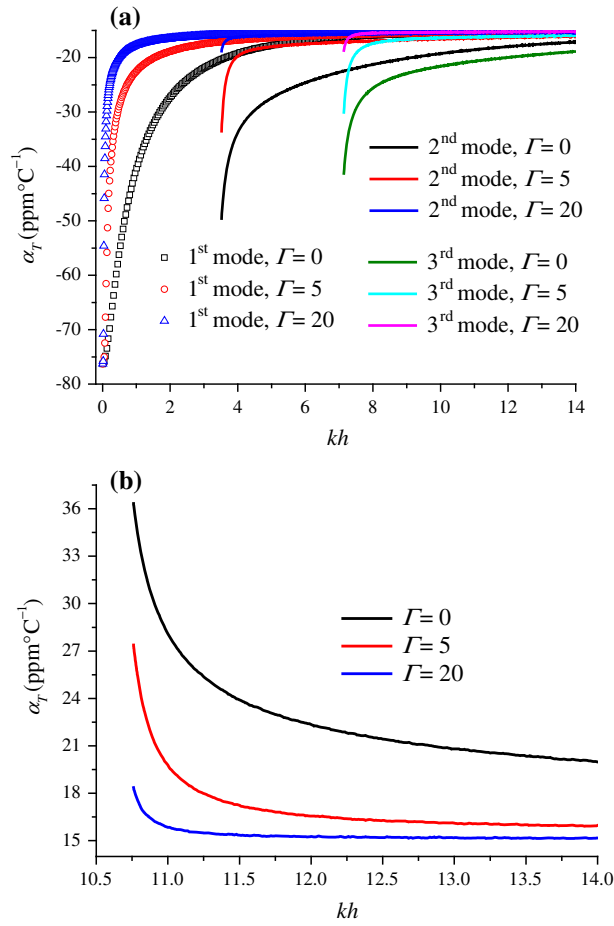


**Fig. 5** The TCD of SH waves as a function of the non-dimensional layer thickness  $kh$  when the upper surface is electrically shorted. **a** The first three modes and **b** the fourth mode

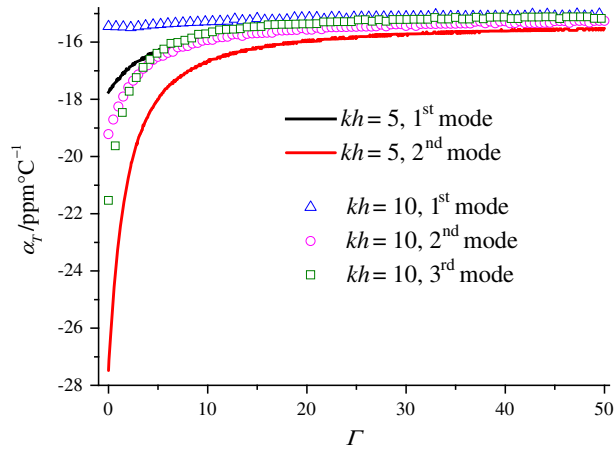


**Fig. 6** The TCD under different modes as a function of the non-dimensional interface parameter  $\Gamma$  when the upper surface is electrically shorted

Only the mass density of the layer, and not its elastic properties, should affect the SH wave, which requires the stress boundary condition at  $x_2 = -h$ , as follows [41]:

$$\sigma_{32}(-h) = -\rho' H \ddot{u}(-h). \tag{28}$$

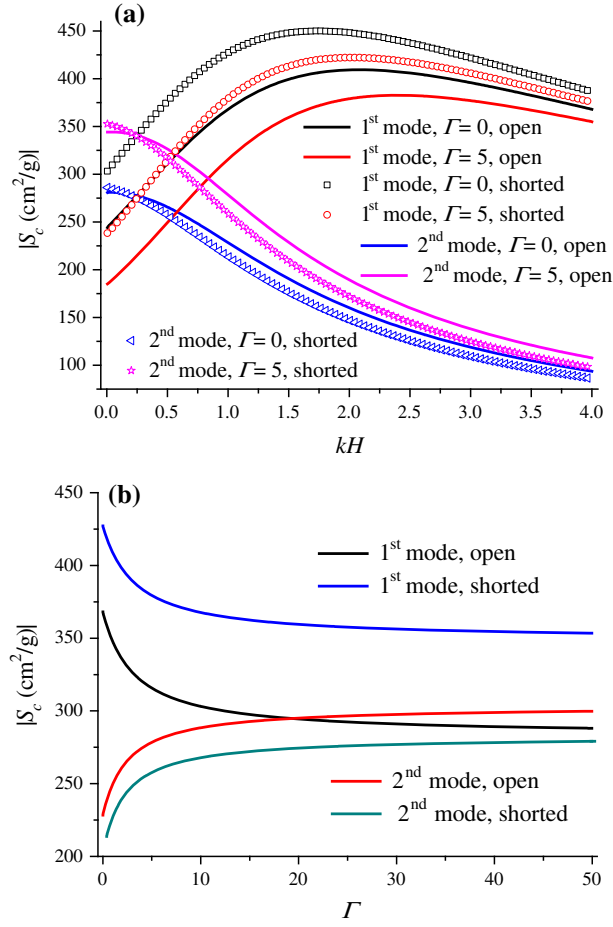


**Fig. 7** The mass loading sensitivity  $S_c$  under different modes ( $kh = 5$ ): **a** with the non-dimensional additional mass layer thickness  $kH$  ( $\Gamma = 0, 5$ ) and **b** with the non-dimensional interface parameter  $\Gamma$  ( $kh = 1$ )

The phase velocity equation of SH waves propagating in the structure with an additional silicon layer on top can be obtained as follows:

$$\begin{aligned}
 & 2k_e^2 b \left[ \frac{1}{\cosh(kbh) \cosh(kh)} - 1 \right] + (k_e^4 + b^2) \tanh(kbh) \tanh(kh) \\
 & + \left[ \frac{\mu b'}{\bar{c}_{44} (1 + b' \Gamma)} - \frac{\rho' c^2 (kH)}{\bar{c}_{44}} \right] [b \tanh(kh) - k_e^2 \tanh(kbh)] \\
 & - \frac{\mu b'}{\bar{c}_{44} (1 + b' \Gamma)} \frac{\rho' c^2 (kH)}{\bar{c}_{44}} \tanh(kbh) \tanh(kh) = 0, \quad (c < c_{\text{layer}} < c_{\text{sub}}), \quad (29.1)
 \end{aligned}$$

$$\begin{aligned}
 & 2k_e^2 b \left[ \frac{1}{\cos(kbh) \cosh(kh)} - 1 \right] + (k_e^4 - b^2) \tan(kbh) \tanh(kh) \\
 & + \left[ \frac{\mu b'}{\bar{c}_{44} (1 + b' \Gamma)} - \frac{\rho' c^2 (kH)}{\bar{c}_{44}} \right] [b \tanh(kh) - k_e^2 \tan(kbh)] \\
 & - \frac{\mu b'}{\bar{c}_{44} (1 + b' \Gamma)} \frac{\rho' c^2 (kH)}{\bar{c}_{44}} \tan(kbh) \tanh(kh) = 0, \quad (c < c_{\text{layer}} < c_{\text{sub}}) \quad (29.2)
 \end{aligned}$$

for electrically shorted cases, and:

$$\left[ \frac{\rho' c^2 (kH)}{\bar{c}_{44}} - b \tanh(kbh) \right] - \left[ 1 - \frac{\rho' c^2 (kH)}{\bar{c}_{44} b} \tanh(kbh) \right] \left[ \frac{\mu b'}{\bar{c}_{44} (1 + b' \Gamma)} - k_e^2 \tanh(kh) \right] = 0, \quad (c < c_{\text{layer}} < c_{\text{sub}}), \quad (30.1)$$

$$\left[ \frac{\rho' c^2 (kH)}{\bar{c}_{44}} + b \tan(kbh) \right] - \left[ 1 - \frac{\rho' c^2 (kH)}{\bar{c}_{44} b} \tan(kbh) \right] \left[ \frac{\mu b'}{\bar{c}_{44} (1 + b' \Gamma)} - k_e^2 \tanh(kh) \right] = 0, \quad (c < c_{\text{layer}} < c_{\text{sub}}) \quad (30.2)$$

for electrically open cases. Considering the additional mass layer is very thin, the electric potential in it has been ignored in the present contribution. If no additional mass layer exists (i.e.,  $H = 0$ ), then Eqs. (29) and (30) have the same expressions as Eqs. (18) and (20).

An imperfect interface and electrical boundary conditions have a significant effect on mass loading sensitivity, as shown in Fig. 7. In general, mass loading sensitivity is negative because the additional layer increases the total mass of the structure. In this study, we discuss its absolute value in Fig. 7. The imperfect interface reduces the sensitivity of the first mode and increases that of higher modes. When the interface parameter  $\Gamma$  is sufficiently large, sensitivity does not change. By choosing an appropriate thickness for the additional mass layer of the first mode with a particular interface, mass loading sensitivity achieves a maximum value.

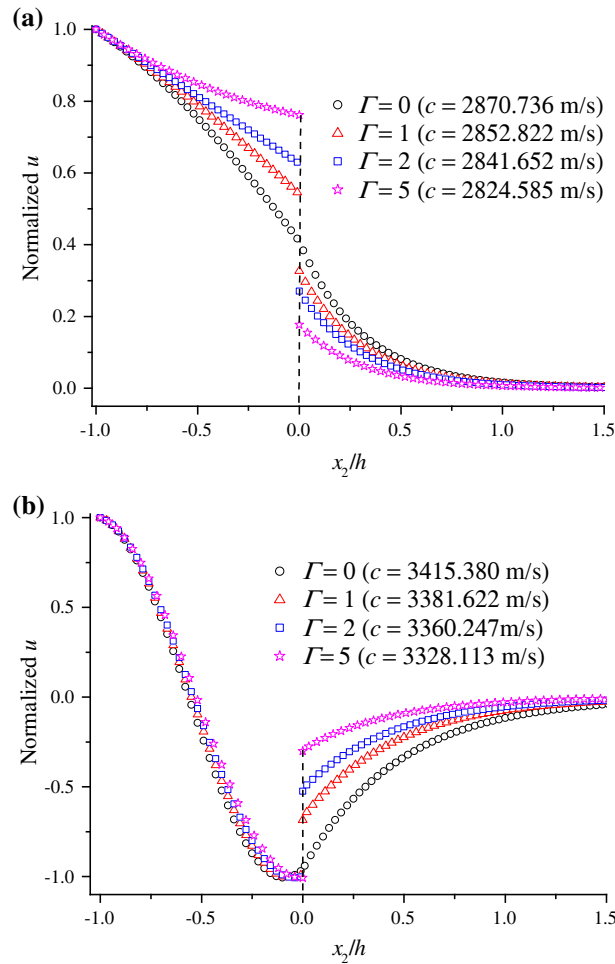


**Fig. 8** The displacement distribution along the thickness direction for selected interface parameters when the upper surface is electrically shorted ( $kh = 5$ ). **a** The first mode and **b** the second mode

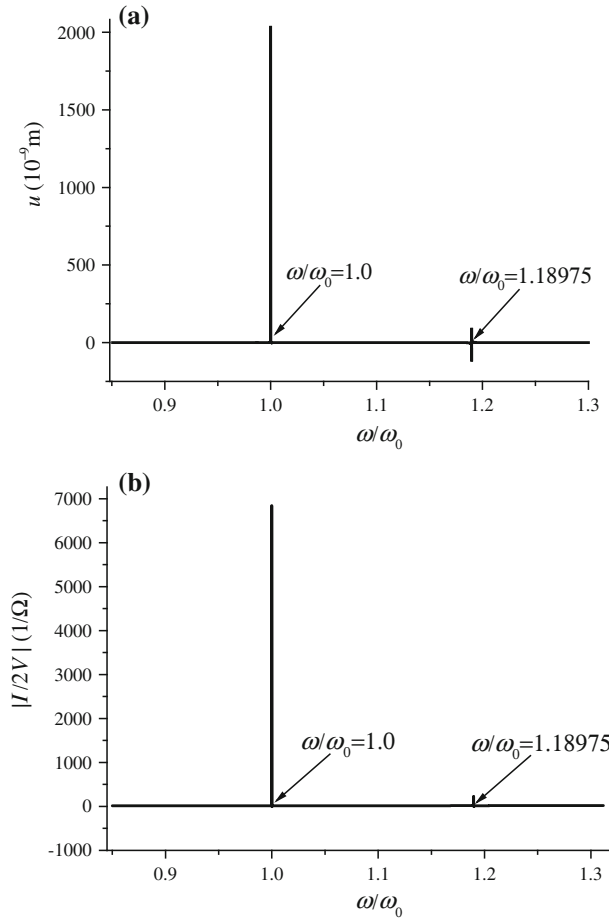


**Fig. 9** The resonances of an excited displacement signal in the substrate at  $x_2 = 0$  and the input admittance in the piezoelectric layer versus the driving frequency when the interface is perfect. **a** The displacement signal  $u$  and **b** the input admittance  $|I/2V|$

For example, a perfectly bonded interface has the largest sensitivity value at  $kH = 2.1$  when the upper layer is electrically open. If the thickness is smaller than this critical value, then the change in phase velocity is relatively small, thus leading to an inferior sensitivity. Sensitivity begins to decrease with increments of  $H$  after it reaches its maximum because the average acoustic flow power descends in layers. Moreover, a thick mass layer increases stiffness, thus causing an inaccurate velocity shift. If the additional mass layer is relatively thick, not only the inertial effect, but also its stiffness effect should be included, and the boundary conditions in Eq. (28) should be improved correspondingly.

### 3.5 Displacement distribution

Figure 8 shows the distribution of the relative amplitude of the mechanical displacement  $u$  along the thickness direction for selected interface parameters. Displacement is normalized such that its value at the excitation position (i.e.,  $x_2 = -h$ ) is equal to one. Mechanical displacement tends to be zero in the substrate for an electrical short circuit, which indicates that most of the energy of SH waves is concentrated in the piezoelectric layer and in the upper surface of the substrate. This condition explains the concept of SAW. The first and second modes have zero and one nodal points along the plate thickness, respectively. Displacement is continuous along the perfect interface. However, the perfect interface breaks its continuity that is caused by the boundary condition at the joint (Eq. (13)). The shear-lag model adopted in the present study is based on the assumption that the interface can be regarded as a layer that geometrically has a zero thickness, but still has elasticity and interface elastic strain energy. A weak interface also causes a large displacement separation, as shown in Fig. 8.

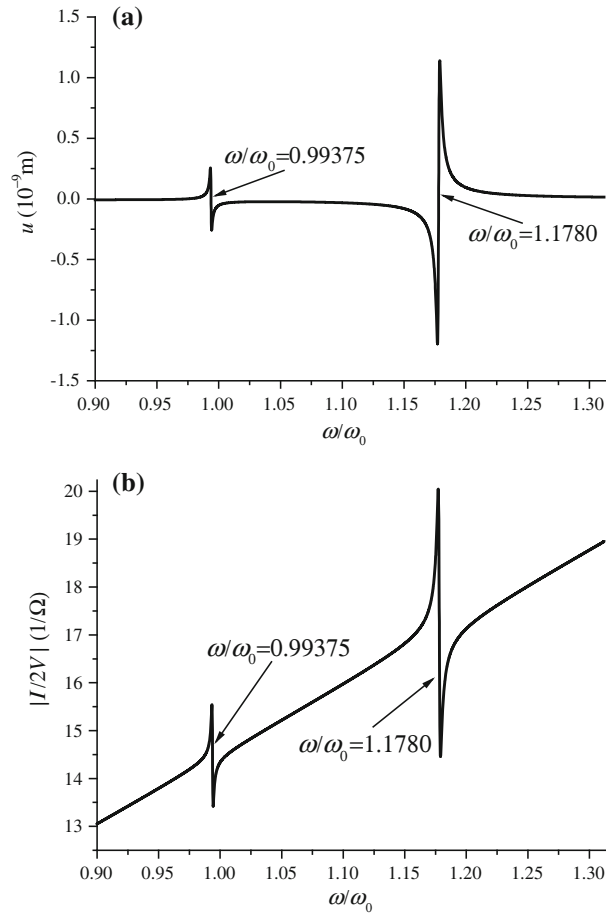


**Fig. 10** The resonances of an excited displacement signal in the substrate at  $x_2 = 0$  and the input admittance in the piezoelectric layer versus the driving frequency with the interface parameters  $\Gamma_1 = 1$  and  $\Gamma_2 = 0.1$ . **a** The displacement signal  $u$  and **b** the input admittance  $|I/2V|$

#### 4 Forced shear horizontal vibration caused by external voltage

In this section, we focus on the effect of an imperfect interface on forced SH or anti-plane vibration excited by an external voltage. SH waves (i.e., Love waves) are generally excited by two separated interdigital electrodes [7]. In this study, we use the voltage imposed on the upper and bottom surfaces of the piezoelectric layer instead of interdigital electrodes. The external voltage is related to the external frequency and is also a harmonic function of time and the coordinates. This electrical boundary condition is sometimes difficult to achieve in practice. However, investigating and understanding the effect of an imperfect interface on the characteristics of forced vibration are advantageous. The solution is obtained as shown above, such as in Eq. (15). The thickness layer is fixed at  $h = 0.5$  mm, and the wave number is  $k = 10,000$   $\text{m}^{-1}$ . At present, the SH wave velocities are  $c_0 = 2,870.736$   $\text{m s}^{-1}$  and  $c_1 = 3,415.380$   $\text{m s}^{-1}$ , as obtained from Fig. 2.  $\omega_0 = kc_0$  is introduced for convenience. Given that the speed of an SH wave is smaller than the bulk shear velocity of the substrate, the external frequency changes within the range of  $0 < \omega < kc_{\text{sub}}$ .

The free charge density on the upper electrode at  $x_2 = -h$  and the density of the current flowing into this electrode are given by the following:

$$Q = -D_2 = \varepsilon_{11}k [-B_1 \sinh(kh) + B_2 \cosh(kh)] \exp[i(kx_1 - \omega t)], \quad (31)$$

$$I = \dot{Q} = -i\omega\varepsilon_{11}k [-B_1 \sinh(kh) + B_2 \cosh(kh)] \exp[i(kx_1 - \omega t)], \quad (32)$$

respectively.

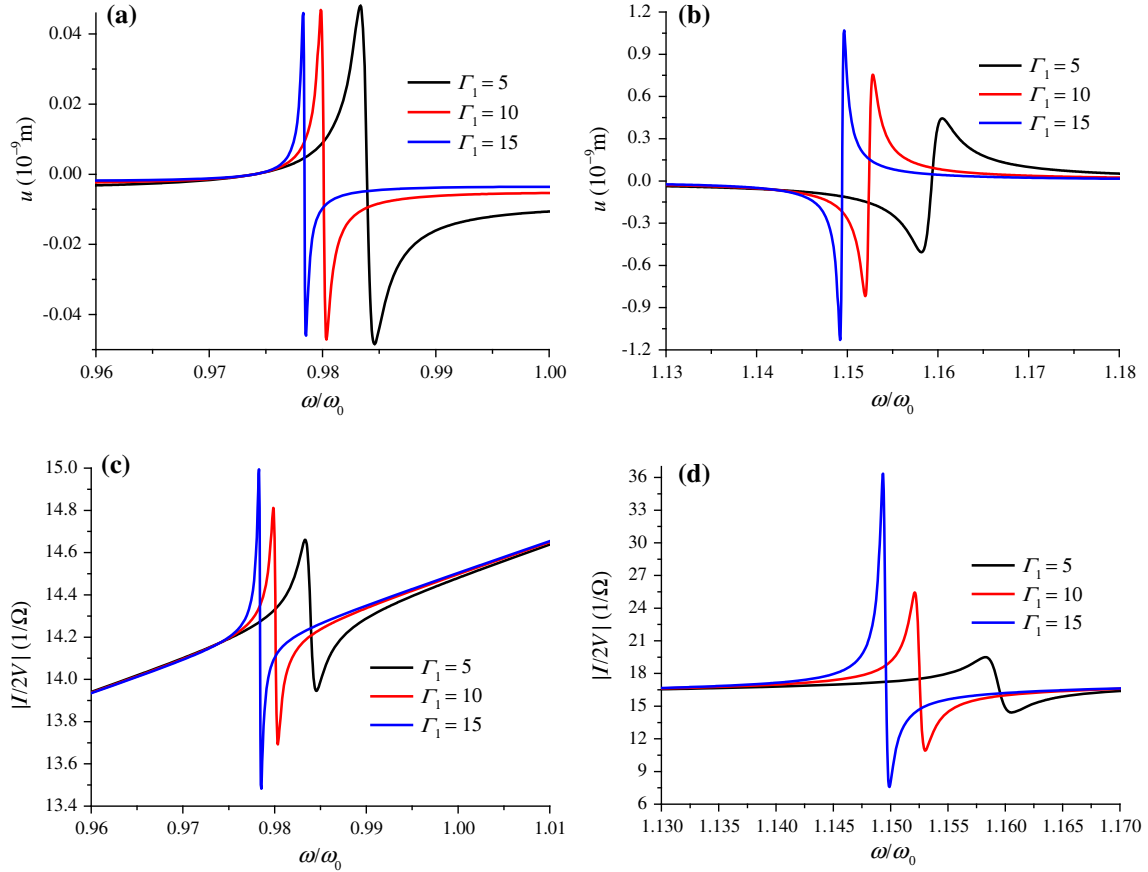


**Fig. 11** The excited displacement signal in the substrate at  $x_2 = 0$  and the input admittance in the piezoelectric layer versus the driving frequency for selected  $\Gamma_1$  ( $\Gamma_2 = 0.5$ ). **a** The displacement  $u$  of the first resonance, **b** the displacement  $u$  of the second resonance, **c** the input admittance  $|I/2V|$  of the first resonance, and **d** the input admittance  $|I/2V|$  of the second resonance

The frequency-dependent admittance  $A$  of the structure per unit electrode area can then be determined from [42]:

$$A = I / (2V). \quad (33)$$

Considering the viscoelasticity of the imperfect interface, we use a complex interface stiffness with an imaginary part that describes interface damping. Given  $R = R_1 + iR_2$ , where both  $R_1$  and  $R_2$  are real. Hence,

$$\Gamma = \Gamma_1 - i\Gamma_2 = \frac{\mu k}{R_1 + iR_2} = \frac{\mu k}{|R|^2} (R_1 - iR_2), \quad (34)$$

where  $\Gamma_1$  and  $\Gamma_2$  are real.  $\Gamma_1$  corresponds to the flexibility of the interface, whereas  $\Gamma_2$  is the viscoelastic parameter. Hence,  $\Gamma_1 = \Gamma_2 = 0$  corresponds to the perfect interface.

Figure 9 shows the excited displacement signal  $u$  at the surface of the  $\text{SiO}_2$  substrate and the input admittance  $|I/2V|$  versus the driving frequency when the sensitive layer is perfectly bonded to the half-space. It should be stressed here that the magnitudes of displacement and input admittance are not zero when the driving frequency is not the resonant frequency. For instance, when external frequency satisfies  $\omega = 0.90\omega_0$ , the amplitude of the excited displacement is  $9.148 \times 10^{-3}$  nm, and if  $\omega = 0.990\omega_0$ , the amplitude will be 0.414 nm. The corresponding magnitude of displacement is  $2.0415 \mu\text{m}$  when the structure is driven in resonant frequency ( $\omega = \omega_0$ ) according to our results. As expected, displacement and input admittance assume their own maxima at resonant frequencies, thus indicating that the device is a resonant type operating at a particular frequency. The peak value of the first mode (i.e.,  $\omega = \omega_0$ ) is significantly larger than that of the second mode. For the imperfect interface, the amplitudes of displacement signal and input admittance are reduced evidently, as shown in Figs. 9 and 10. We believe that this scenario is caused by the introduction of the viscoelastic

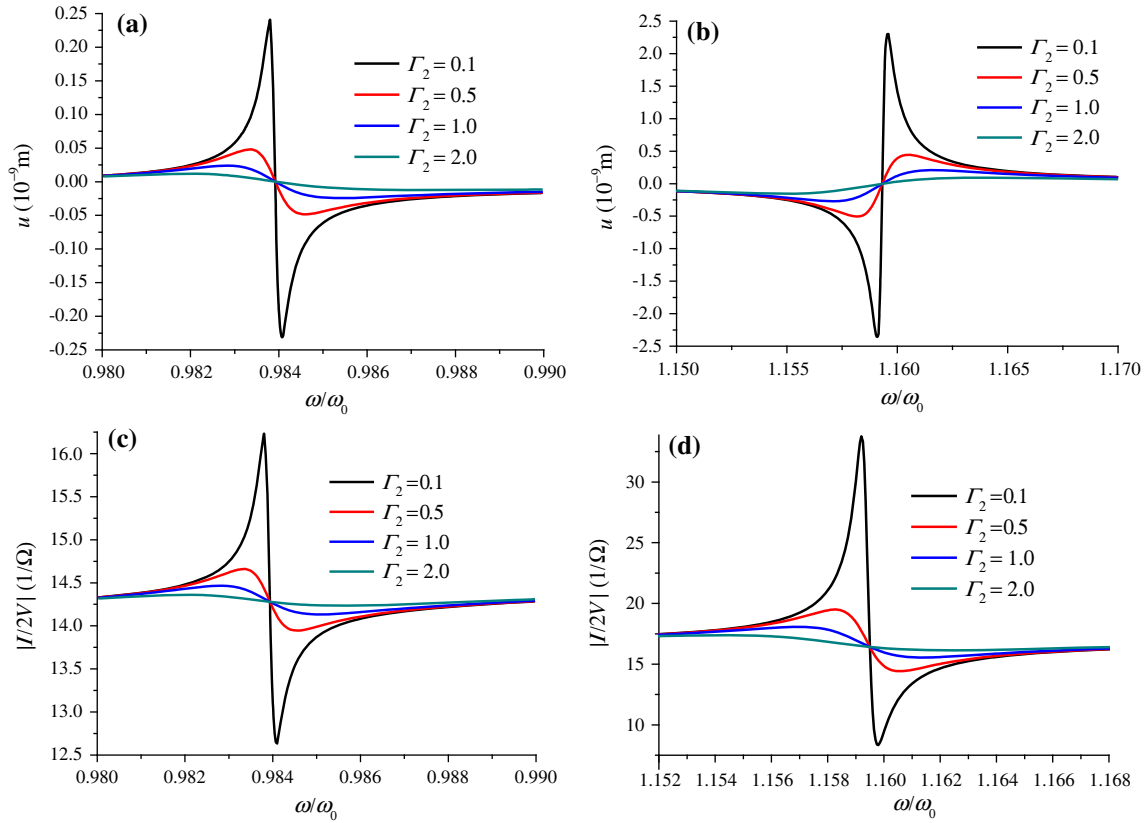


**Fig. 12** The excited displacement signal in the substrate at  $x_2 = 0$  and the admittance in the piezoelectric layer versus the driving frequency for selected  $\Gamma_2$  ( $\Gamma_1 = 5$ ). **a** The displacement  $u$  of the first resonance, **b** the displacement  $u$  of the second resonance, **c** the input admittance  $|I/2V|$  of the first resonance, and **d** the input admittance  $|I/2V|$  of the second resonance

parameter  $\Gamma_2$ . Moreover, the imperfect interface decreases the stiffness of the entire structure, thus reducing resonant frequencies. The resonant amplitude of the second resonance is determined to be larger than that of the first. In particular, excited displacement and input admittance are affected significantly by the imperfect interface.

The effects of the interface parameters  $\Gamma_1$  and  $\Gamma_2$  on the local performance of the surface acoustic device near the resonances are shown in Figs. 10 and 11, respectively. Resonant frequency is sensitive to the interface parameter  $\Gamma_1$ , but insensitive to  $\Gamma_2$ .  $\Gamma_1$  decreases resonant frequency and has a significant effect on the amplitudes of excited displacement and input admittance. For the displacement of the first mode,  $\Gamma_1$  reduces its amplitude when resonance occurs. However, a large  $\Gamma_1$  results in the amplification of the displacement signal of the second resonance (Fig. 11a, b). Furthermore, this parameter also increases the amplitude of the input admittance of resonances, as shown in Fig. 11c, d. As a viscoelastic parameter,  $\Gamma_2$  that represents interface damping does not affect the resonance frequency. This parameter only significantly affects the amplitudes of displacement and input admittance. In particular, a large  $\Gamma_2$  expectedly causes small amplitude (Fig. 12).

## 5 Conclusions

The shear-lag interface model is used to simulate the effect of an imperfect interface on SH wave propagation in a piezoelectric composite structure. Overall, the weak interface evidently affects performance, including phase velocity, electromechanical coupling factor, TCD, mass loading sensitivity, and displacement distribution along the thickness direction. When the interface is imperfect, the minimum value of phase velocity of the first mode can achieve a value which is smaller than the B–G wave velocity in the piezoelectric layer, which is totally different from the case of perfect interface. Moreover, the presence of a weak interface is beneficial because it improves the energy transformation ratio, temperature stability, and mass sensitivity of SAW devices. For forced vibration, the viscoelasticity damping of the interface is introduced to discuss resonant

frequency, excited displacement signal, and input admittance compared with those of a perfect interface. This viscoelasticity parameter only significantly affects the amplitudes of displacement and input admittance, and has no relationship with resonant frequencies. The theoretical and numerical results can provide guidance in designing piezoelectric SAW devices when an imperfect interface is present.

**Acknowledgments** The National Natural Science Foundation of China (No. 11272247) and the National 111 Project of China (No. B06024) are gratefully acknowledged for their financial support.

## References

1. Love, A.E.H.: *Some Problems of Geodynamics*. Cambridge University Press, London (1911)
2. Bleustein, J.L.: A new surface wave in piezoelectric material. *Appl. Phys. Lett.* **13**, 412–413 (1968)
3. Gulyaev, Y.V.: Electroacoustic surface waves in solids. *JETP Lett.* **9**, 37–38 (1969)
4. Gulyaev, Y.V.: Review of shear surface acoustic waves in solids. *IEEE Trans. Ultrason. Ferroelectr. Freq. Control* **45**, 935–938 (1998)
5. Nakamura, K.: Shear-horizontal piezoelectric surface acoustic waves. *Jpn. J. Appl. Phys.* **46**, 4421–4427 (2007)
6. Collet, B., Destrade, M.: Explicit secular equations for piezoacoustic surface waves: Shear-horizontal modes. *J. Acoust. Soc. Am.* **116**, 3432–3442 (2004)
7. Wang, Q., Varadan, V.K.: Wave propagation in piezoelectric coupled plates by use of interdigital transducer: part 1. Dispersion characteristics. *Int. J. Solids Struct.* **39**, 1119–1130 (2002)
8. Melkumyan, A.: Twelve shear surface waves guided by clamped/free boundaries in magneto-electro-elastic materials. *Int. J. Solids Struct.* **44**, 3594–3599 (2007)
9. Yang, J.S.: Love waves in piezoelectromagnetic materials. *Acta Mech.* **168**, 111–117 (2004)
10. Son, M.S., Kang, Y.J.: The effect of initial stress on the propagation behavior of SH waves in piezoelectric coupled plates. *Ultrasonics* **51**, 489–495 (2011)
11. Dutta, S.: On the propagation of Love waves in a non-homogeneous internal stratum of finite depth lying between two semi-infinite isotropic media. *Pure Appl. Geophys.* **55**, 31–36 (1963)
12. Eskandari, M., Shodja, H.M.: Love waves propagation in functionally graded piezoelectric materials with quadratic variation. *J. Sound Vib.* **33**, 195–204 (2008)
13. Du, J.K., Xian, K., Wang, J., Yong, Y.K.: Love wave propagation in piezoelectric layered structure with dissipation. *Ultrasonics* **49**, 281–286 (2009)
14. Kielczynski, P., Szalewski, M., Balcerzak, A.: Effect of a viscous liquid loading on Love wave propagation. *Int. J. Solids Struct.* **49**, 2314–2319 (2012)
15. Chattopadhyay, A., De, R.K.: Love type waves in a porous layer with irregular interface. *Int. J. Eng. Sci.* **21**, 1295–1303 (1983)
16. Termonia, Y.: Fibre coating as a means to compensate for poor adhesion in fibre-reinforced materials. *J. Mater. Sci.* **25**, 103–106 (1990)
17. Schoenberg, M.: Elastic wave behavior across linear slip interfaces. *J. Acoust. Soc. Am.* **68**, 1516–1521 (1980)
18. Otero, J.A., Rodríguez-Ramos, R., Bravo-Castillero, J., Monsivais, G.: Interfacial waves between two piezoelectric half-spaces with electro-mechanical imperfect interface. *Philos. Mag. Lett.* **92**, 534–540 (2012)
19. Chen, W.Q., Lee, K.Y.: Exact solution of angle-ply piezoelectric laminates in cylindrical bending with interfacial imperfections. *Compos. Struct.* **65**, 329–337 (2004)
20. Jin, F., Kishimoto, K., Inoue, H., Tateno, T.: Experimental investigation on the interface properties evaluation in piezoelectric layered structures by Love waves propagation. *Key Eng. Mater.* **297–300**, 807–812 (2005)
21. Lavrentyev, A.I., Rokhlin, S.I.: Ultrasonic spectroscopy of imperfect contact interfaces between a layer and two solids. *J. Acoust. Soc. Am.* **103**, 657–664 (1998)
22. Nagy, P.B.: Ultrasonic classification of imperfect interfaces. *J. Nondestruct. Eval.* **11**, 127–139 (1992)
23. Joshi, S.P.: Non-linear constitutive relations for piezoceramic materials. *Smart Mater. Struct.* **1**, 80–83 (1992)
24. Liu, J.X., Wang, Y.L., Wang, B.L.: Propagation of shear horizontal surface waves in a layered piezoelectric half-space with an imperfect interface. *IEEE Trans. Ultrason. Ferroelectr. Freq. Control* **57**, 1875–1879 (2010)
25. Qian, Z.H., Jin, F., Hirose, S.: A novel type of transverse surface wave propagating in a layered structure consisting of a piezoelectric layer attached to an elastic half-space. *Acta Mech. Sinica* **26**, 417–423 (2010)
26. Zhou, Y.Y., Lv, C.F., Chen, W.Q.: Bulk wave propagation in layered piezomagnetic/piezoelectric plates with initial stresses or interface imperfections. *Compos. Struct.* **94**, 2345–2736 (2012)
27. Curtis, R.G., Redwood, M.: Transverse surface waves on a piezoelectric material carrying a metal layer of finite thickness. *J. Appl. Phys.* **44**, 2002–2007 (1973)
28. Achenbach, J.D.: *Wave Propagation in Elastic Solids*. North-Holland, New York (1973)
29. Abdalla, A.N., Alsheikh, F., AlHossain, A.Y.: Effect of initial stresses on dispersion relation of transverse waves in a piezoelectric layered cylinder. *Mater. Sci. Eng. B-Adv.* **162**, 147–154 (2009)
30. Krishnamoorthya, S., Iliadisa, A.A.: Development of high frequency ZnO/SiO<sub>2</sub>/Si Love mode surface acoustic wave devices. *Solid State Electron.* **50**, 1113–1118 (2006)
31. Su, J., Kuang, Z.B., Liu, H.: Love wave in ZnO/SiO<sub>2</sub>/Si structure with initial stresses. *J. Sound Vib.* **286**, 981–999 (2005)
32. Wang, Q., Quek, S.T., Varadan, V.K.: Love waves in piezoelectric coupled solid media. *Smart Mater. Struct.* **10**, 380–388 (2001)
33. Dvoeshertov, M.Y., Cherednik, V.I., Chirimanov, A.P.: Electroacoustic Lamb waves in piezoelectric crystal plates. *Acoust. Phys.* **50**, 512–517 (2004)
34. Jakoby, B., Vellekoop, M.J.: Properties of Love waves: applications in sensors. *Smart Mater. Struct.* **6**, 668–679 (1997)

35. Milsom, R.F., Redwood, M.: Piezoelectric coupling coefficient of Bleustein–Gulyaev waves. *Electron. Lett.* **6**, 665–666 (1970)
36. Tomar, M., Gupta, V., Mansingh, A., Sreenivas, K.: Temperature stability of *c*-axis oriented LiNbO<sub>3</sub>/SiO<sub>2</sub>/Si thin film layered structures. *J. Phys. D-Appl. Phys.* **34**, 2267–2273 (2001)
37. Chen, X., Liu, D.L.: Temperature stability of ZnO-based Love wave biosensor with SiO<sub>2</sub> buffer layer. *Sensor Actuat. A-Phys.* **156**, 317–322 (2009)
38. Nishida, T., Ibrahim, R.C., Horiuchi, T., Shioasaki, T., Matsushige, K.: Theoretical study on surface acoustic wave characteristics of LiNbO<sub>3</sub> films on sapphire substrates. *Jpn. J. Appl. Phys.* **36**, 6077–6082 (1997)
39. Tomar, M., Gupta, V., Sreenivas, K., Mansingh, A.: Temperature stability of ZnO thin film SAW device on fused quartz. *IEEE Trans. Dev. Mater. Reliab.* **5**, 494–500 (2005)
40. Chen, X., Liu, D.L., Chen, J.S., Wang, G.L.: The effect of a SiO<sub>2</sub> layer on the performance of a ZnO-based SAW device for high sensitivity biosensor applications. *Smart Mater. Struct.* **18**, 115021 (2009)
41. Bovik, P.: A comparison between the Tiersten model and O(H) boundary conditions for elastic surface waves guided by thin layers. *J. Appl. Mech.* **63**, 162–167 (1996)
42. Xu, L.M., Geng, Y.L., Zhang, Y., Fan, H.: Power transmission through an unbounded elastic plate using a finite piezoelectric actuator and a finite piezoelectric power harvester. *Int. J. Appl. Electromagn.* **29**, 145–156 (2009)